International Journal of Mass Spectrometry 297 (2010) 131–138

Contents lists available at ScienceDirect

International Journal of Mass Spectrometry

journal homepage: www.elsevier.com/locate/ijms

Vibrational signatures of zwitterionic and charge-solvated structures for alkaline earth-tryptophan dimer complexes in the gas phase

Warren K. Mino Jr.[a], Jan Szczepanski[a], W. Lee Pearson[a], David H. Powell[a], Robert C. Dunbar[b], John R. Eyler[a], Nick C. Polfer[a,*]

[a] Department of Chemistry, University of Florida, P.O. Box 117200 Gainesville, FL 32611-7200, United States
[b] Department of Chemistry, Case Western Reserve University, 10900 Euclid Avenue Cleveland, OH 44106-7078, United States

ARTICLE INFO

Article history:
Received 6 April 2010
Received in revised form 17 July 2010
Accepted 26 July 2010
Available online 6 August 2010

Keywords:
Ion spectroscopy
IR-MPD
Zwitterion
OPO
Tryptophan
Alkaline earth metals

ABSTRACT

Infrared multiple-photon dissociation (IR-MPD) spectra in the N–H and O–H stretching region (3000–3700 cm^{-1}) are reported for gas-phase monomeric M^{2+}Trp and dimeric $M^{2+}Trp_2$ complexes (where M = Mg, Ca, Sr, and Ba). The spectra are obtained by irradiating the complexes in the Penning trap of a Fourier transform ion cyclotron resonance (FT-ICR) mass spectrometer, using a tunable continuous-wave (cw) optical parametric oscillator (OPO) laser in combination with a fixed wavelength CO_2 laser (10.6 μm). These spectra are compared with previously recorded mid-IR-MPD spectra, using the free electron laser FELIX, and are interpreted based on harmonic frequency calculations performed with density-functional theory (DFT). The experimental spectra show that a simple assignment of bands can be made to distinguish zwitterionic (ZW) from charge solvation (CS) complexes. In particular, the carboxylic acid O–H stretch at ~3550 cm^{-1} identifies the presence of a CS structure, whereas the NH_3^+ antisymmetric stretching mode in the 3150–3375 cm^{-1} range is diagnostic of a ZW structure. For the monomeric Ba^{2+}Trp complex, exclusively the ZW structure is observed. Conversely, for the dimeric complexes of $M^{2+}Trp_2$ (M = Sr and Ba) merely CS/CS geometries are confirmed. Surprisingly, for smaller alkaline earth metal dications (M = Mg and Ca), the IR-MPD spectra are consistent with the presence of mixed CS/ZW dimers. This is contrary to most previous trends for alkali metals, where larger cations typically favor ZW stabilization.

1. Introduction

Tryptophan–metal cation interactions are known to play important roles in biology. For instance, tryptophan is present in the entrance/exit [1] and selectivity filter [2] regions of select ion channel proteins. Specifically, tryptophan is believed to be involved with the gating function of the gramicidin-A [3], and gramicidin-S ion channels [4,5], as well as the Ca^{2+} channel in N-methyl-D-aspartate [6].

Gas-phase studies can characterize inherent amino acid interactions with metal cations in the absence of solution effects. Tryptophan offers multiple binding patterns, such as electrostatic interactions with the three Lewis-basic heteroatoms (amino N and carboxylic acid O's) and a cation–π interaction with the aromatic indole side chain. In addition, the amino acid has the ability to bind in the zwitterionic (ZW) or charge-solvated (CS, non-zwitterionic) forms, presenting numerous possible conformations. Figs. 1 and 2 show the most stable binding motifs for the monomer Ba^{2+}Trp and dimer $M^{2+}Trp_2$ complexes calculated with density-functional theory (DFT), and the same nomenclature is employed herein as described by Dunbar et al. [7]. Briefly, C1 denotes a CS tryptophan configuration and Z1–Z4 denote the ZW form.

Infrared multiple-photon dissociation (IR-MPD) spectroscopy [8–12] is a powerful tool in distinguishing ZW and CS conformations of amino acids and peptides. The majority of these studies made use of free electrons lasers (FELs), which offer tunability and spectral brightness in the mid-infrared range (500–2000 cm^{-1}). The mid-IR region includes the CS-specific carboxylic acid C=O stretch, as opposed to the ZW-specific antisymmetric carboxylate CO_2^- stretch. A number of studies have shown that singly-charged metal cations complexed with amino acids or small peptides in the gas-phase predominantly exist in the CS form [13–28]. Basic amino acids, such as arginine [13,17,29,30], proline [12], and lysine analogues [31] seem to buck this trend, as well as serine [27] and methionine [32], particularly if bound to larger alkali metals (i.e., Rb^+ and Cs^+). Conversely, divalent metal cations, specifically Ba^{2+}, have been shown to completely stabilize the ZW form of amino acids in the gas phase [33,34]. These studies have since been expanded to dimeric complexes, in the form $M^{2+}Trp_2$ [7]. Other amino acid dimer species that have been studied include

* Corresponding author. Tel.: +1 352 392 0492; fax: +1 352 392 0872.
E-mail address: polfer@chem.ufl.edu (N.C. Polfer).

1387-3806/$ – see front matter © 2010 Elsevier B.V. All rights reserved.
doi:10.1016/j.ijms.2010.07.026

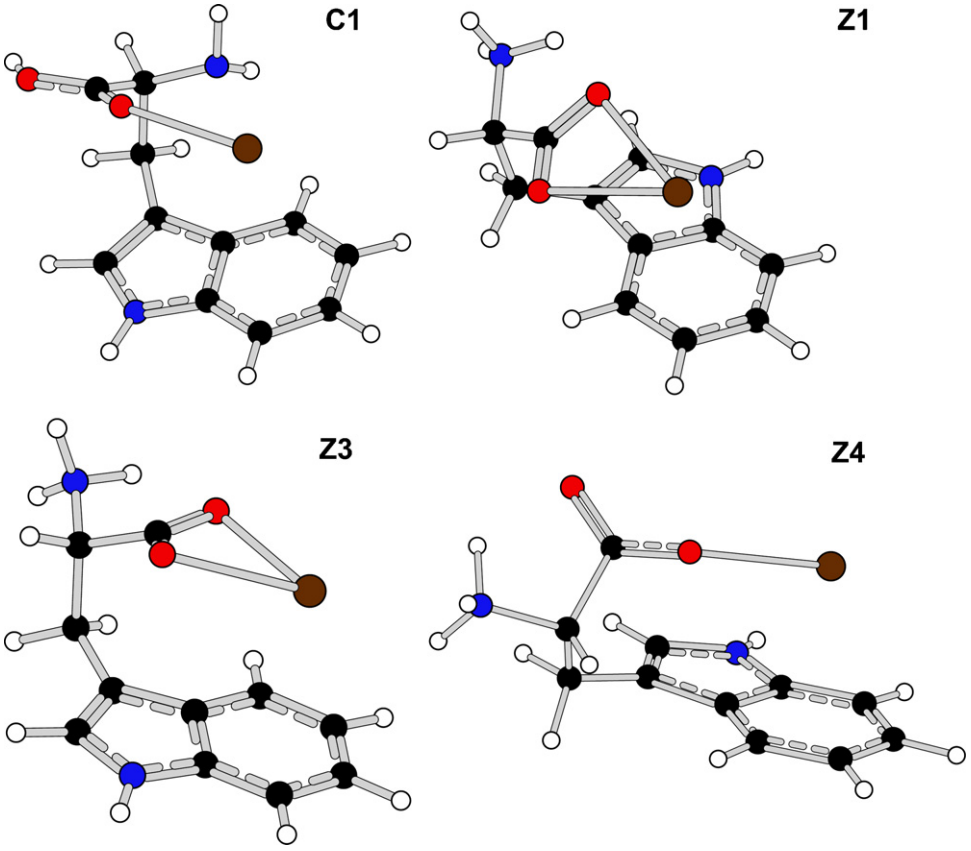

Fig. 1. Four of the lowest-energy calculated structures for the Ba^{2+}Trp complex. C1 denotes a charge-solvated (CS) configuration and Z1, Z3, and Z4 denote the zwitterionic (ZW) configuration. The numbers represent different conformers in each configuration.

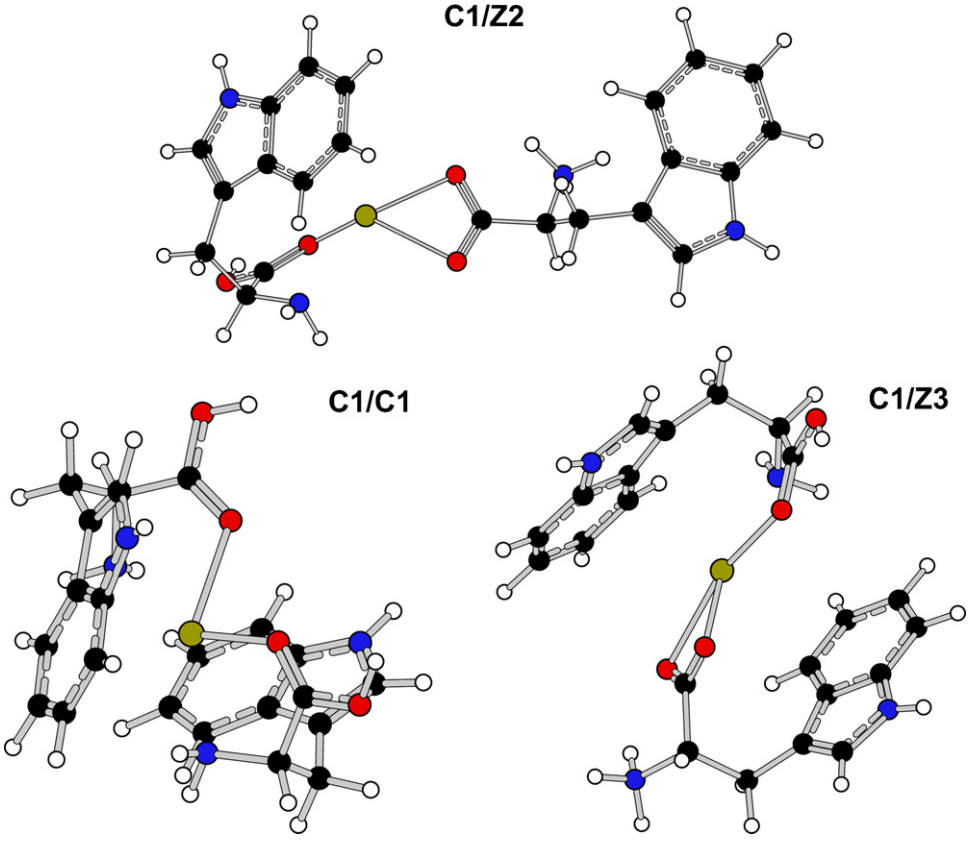

Fig. 2. Three lowest-energy calculated structures for the $M^{2+}Trp_2$ complex, where M is Mg, Ca, Sr, and Ba. C1 denotes a charge-solvated configuration and Z2 and Z3 denote the zwitterionic (ZW) configuration. The numbers represent different conformers in each configuration.

proton-bound glycine, alanine and proline dimers [35,36]. Compared to monomeric complexes, dimer mid-IR-MPD spectra exhibit increased spectral congestion, thus complicating interpretation.

Initial studies by Jockusch et al. [13] proposed that the carboxylate group solvates the larger alkali metals more effectively, thus promoting the ZW form. This was later confirmed by IR-MPD spectroscopy [17,29]. IR-MPD spectroscopy studies on alkali–metal chelated serine and methionine by Armentrout and co-workers displayed similar trends [27,32]. For tryptophan monomers, Dunbar et al. predicted that metal dications favor the ZW form, provided that the binding energy is relatively low. This suggested that Ca^{2+}, Sr^{2+} and Ba^{2+} favor the ZW form, whereas Mg^{2+} does not. Studies by Bush et al. [37] on barium-chelated arginine, glutamine, proline, serine and valine, showed that all preferentially formed the ZW.

Here, the use of a bench-top continuous-wave (cw) optical parametric oscillator (OPO) laser to differentiate between CS and ZW structures for $M^{2+}Trp_2$ complexes by irradiating the O–H and N–H stretching region (3000–3700 cm^{-1}) is demonstrated. Despite the usefulness of this region for CS vs. ZW differentiation exemplified by the CS-diagnostic carboxylic acid O–H stretch and the ZW-specific NH_3^+ stretching modes, relatively few studies have made use of OPO-lasers for this purpose [34,38,39]. Over the years, most infrared photodissociation studies involving OPO-lasers have been carried out on either Van der Waals complexes [40–46], or on solvated clusters [10,47], which require low dissociation thresholds. In the infrared-ultraviolet photodissociation scheme pioneered by Rizzo et al. [48], absorption of a UV photon causes photodissociation, whereas prior absorption of an IR photon leads to a dip in the photodissociation yield. The cw OPO laser in our study is capable of inducing covalent bond cleavage, particularly in combination with a higher-power CO_2 laser. The work reported here follows up a recent IR-MPD study on weakly bound carbohydrate–Rb^+ isomers, which exclusively made use of the cw OPO-laser [49]. In terms of the differentiation between ZW and CS, it will be shown that the NH_3^+ and OH vibrational modes are separated by approximately 250–300 cm^{-1} in these complexes, thus allowing a relatively simple assignment of the bands. The O–H and N–H stretching region can therefore be regarded as a 'fingerprint' region for the identification of ZW or CS gas-phase structures of these dimer complexes.

2. Materials and methods

2.1. Materials

Standard solutions of $Mg(NO_3)_2$, $Ca(NO_3)_2$, $Sr(NO_3)_2$, $Ba(NO_3)_2$, and L-Trp (all from Acros Organics) were prepared in HPLC-grade water (Fisher Scientific) at a concentration of 10^{-2} M. The L-Trp solution was then mixed with each of the metal solutions separately in a 1:1 ratio and diluted to yield a final concentration of 10^{-3} M in a 70:30 methanol (Fisher Scientific)/water solution.

2.2. Mass spectrometry and ion spectroscopy

The $Ba^{2+}Trp$ and $M^{2+}Trp_2$ complexes of interest were formed by electrospray ionization (ESI) in a commercial 4.7 T Apex II Fourier transform ion cyclotron resonance (FT-ICR) mass spectrometer (Bruker Daltonics, Billerica, MA). Infrared multiple-photon dissociation (IR-MPD) spectroscopy was performed by irradiating the mass-selected cations in a stepwise fashion with the tunable output (2500–4000 cm^{-1}) of a continuous-wave (cw) periodically poled lithium niobate-optical parametric oscillator (OPO) OS4000 laser (LINOS Photonics, Germany). The IR-MPD spectra were generated by plotting the IR-MPD yield, yield = $-\ln[1-\{\sum Int_{photofragments}/(\sum Int_{photofragments} + Int_{precursor})\}]$, as a function of the OPO idler wavenumber (cm^{-1}).

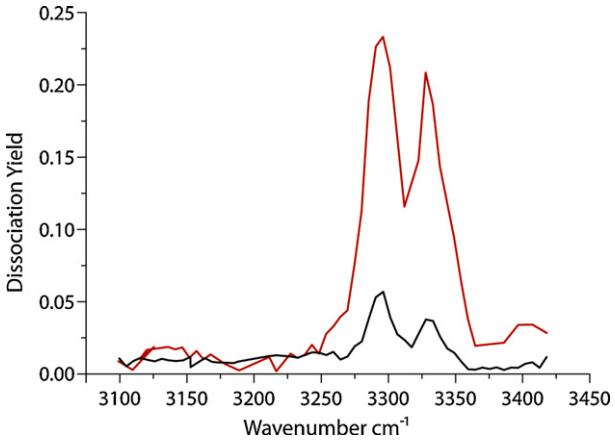

Fig. 3. Comparison of the dissociation yield when irradiating for 10 s with the OPO-laser alone (black) *vs.* sequential irradiation by the OPO for 10 s and CO_2 lasers for 500 ms (red). The overall dissociation yield is increased from 5% to 25% and the signal-to-noise ratio is increased from 13 to 32. (For interpretation of references to color in this figure legend, the reader is referred to the web version of this article.)

The main dissociation pathways observed from the IR-MPD experiments were neutral loss of NH_3 (minor loss of $2NH_3$ only observed in the dimers) and loss of Trp. Relatively long irradiation times (10 s) were required to induce 50–70% photodepletion of strong modes, due to the low power (30–50 mW) of the OPO laser. The laser fluence under these conditions was estimated at 1.2–2 J/cm^2 for a spot size of 0.25 cm^2 (per laser beam), even if the overlap between the ion cloud and the laser beam is unknown. In order to verify laser alignment from day to day, the indole N–H stretching mode for $Ba^{2+}Trp$ served as a useful calibrant peak. OPO-laser irradiation was followed by irradiation at a discrete wavelength (10.6 μm) using a high-power (max power 50 W) CO_2 laser (SYNRAD J48-5W, Mukilteo, WA) to boost the IR-MPD yield, which is particularly useful for weaker vibrational bands. Resonant absorption of multiple photons with the OPO laser results in an increased population of ions at higher internal energies than room temperature, but lower than the dissociation threshold. Irradiation by the higher-power CO_2 laser for 500 ms (~2 W) raises the internal energy of a fraction of those ions above the dissociation threshold, thus inducing photodissociation. The combination of two infrared lasers to photodissociate was first used by Lee and co-workers [50]. Eyler and co-workers later implemented a scheme involving two CO_2 lasers in the Penning trap of an FT-ICR [51]. Here, the approach is demonstrated to improve figures of merit for IR-MPD of the N–H stretching modes of the $Ba^{2+}Trp$ in Fig. 3. The OPO-CO_2 coupled laser irradiation increased the IR-MPD yield from 5% to 25% and increased the signal-to-noise ratio from 13 to 32. Thus, while a considerable fraction of the ions (i.e., 50–70%) dissociate directly from OPO-laser irradiation on stronger vibrational modes, the IR-MPD yield can be markedly increased by the dual OPO-CO_2 laser scheme for weaker modes.

Mechanistic aspects of IR-MPD have been reviewed before [8,9], and will not be explained in detail here. Empirically, it has been observed that IR-MPD intensities can deviate significantly from those of linear absorption spectra; however, interpretation of IR-MPD spectra relies on absorption band positions rather than absorption band intensities. The OPO-CO_2 laser approach described above is employed to ensure weak vibrational bands are observed above the background – since interpretation relies mostly on IR-MPD band positions rather than intensities, the effect of the CO_2 laser on band intensities does not adversely affect the interpretation of the IR-MPD spectra. It is important that no (intense) resonant absorption occurs at the CO_2 fixed wavelength, as this would result in non-selective photodissociation of all ions, regard-

less of OPO irradiation wavelength. Instead, for the OPO-CO_2 laser photodissociation scheme to work, the spectroscopy relies on resonant absorption of the OPO-laser energy to bring ions to a higher density of states, thus allowing for the off-resonant CO_2 laser to selectively photodissociate those ions.

The IR-MPD results in the 3000–3700 cm^{-1} region are contrasted to previously published IR-MPD spectra in the mid-IR-range 600–1800 cm^{-1} [7] using the free electron laser, FELIX, at the FOM Institute for Plasma Physics 'Rijnhuizen' coupled to a home-built FT-ICR mass spectrometer [52]. In that study, complexes were generated by ESI and transferred to the Penning trap and irradiated with the FELIX beam.

2.3. Calculations

Theoretical structures and IR spectra were previously calculated with density-functional theory (DFT), employing the B3LYP functional with a 6-31+g(d,p) basis set and a Stuttgart–Dresden (SDD) relativistic core potential on the metal for Sr and Ba [7] with the Gaussian03 software package [53]. The same nomenclature was employed as in the previous paper by Dunbar et al. [7], except for Z1, which denotes the lowest-energy ZW conformation Ba^{2+}Trp conformer (labeled as SB O/O/Ring) in an earlier study [33]. The SDD core potential has been reported to be adequate for calculating vibrational frequencies and intensities for metal–ion complexes [7,14,15]. The computed vibrational frequencies were scaled [54] by 0.975 and stick spectra were broadened with a Gaussian function to 30 cm^{-1} FWHM (full width at half-maximum). The convoluted spectra were then normalized to integral band intensities in km mol^{-1} for more convenient comparison of vibrational intensities. The zero-point energy (ZPE) corrected energies are shown for comparison in Figs. 4, 6 and 7.

3. Results and discussion

3.1. Ba^{2+} tryptophan monomer complex

In Fig. 4, the IR-MPD spectrum of Ba^{2+}Trp is compared to four of the calculated lowest-energy ZW and CS isomer structures. Three characteristic stretching modes are predicted in the calculated Ba^{2+}Trp IR-MPD spectra (1) O–H stretch from the carboxylic acid terminus, 3525–3625 cm^{-1}, highlighted in blue, (2) N–H stretch from the indole on the tryptophan side chain (this is expected for all structures), 3450–3500 cm^{-1}, highlighted in red (3) N–H stretches from the amine NH_2 or NH_3^+ groups, 3150–3375 cm^{-1}, highlighted in yellow. Note that, although absorption is expected for both CS and ZW structures in the N–H stretching (yellow) region, the spectral brightness of the two CS NH_2 stretches is predicted to be much lower when compared to the ZW NH_3^+ stretches (21 and 19 km mol^{-1} vs. 151 and 101 km mol^{-1}).

Comparison of the experimental IR-MPD Ba^{2+}Trp spectrum with calculated spectra suggests that the complex adopts a ZW structure, based on the lack of an O–H stretching mode and the presence of a doublet feature at 3290 and 3320 cm^{-1}, consistent with the antisymmetric NH_3^+ stretching modes. Among the ZW conformations, Z3 and Z4 predict an intense symmetric NH_3^+ mode (at 3170 cm^{-1} and 3150 cm^{-1}, respectively), while Z1 does not. Clearly, no mode is observed at this position, which suggests that exclusively Z1 is present. Thermochemically, Z3 is slightly favored relative to Z1 (+2 kJ mol^{-1}); however, this is within the error of the calculation. Structurally, Z1 and Z3 differ in the orientation of the indole side-chain. This suggests that both structures cannot interconvert readily and supports the hypothesis that exclusively Z1 is present.

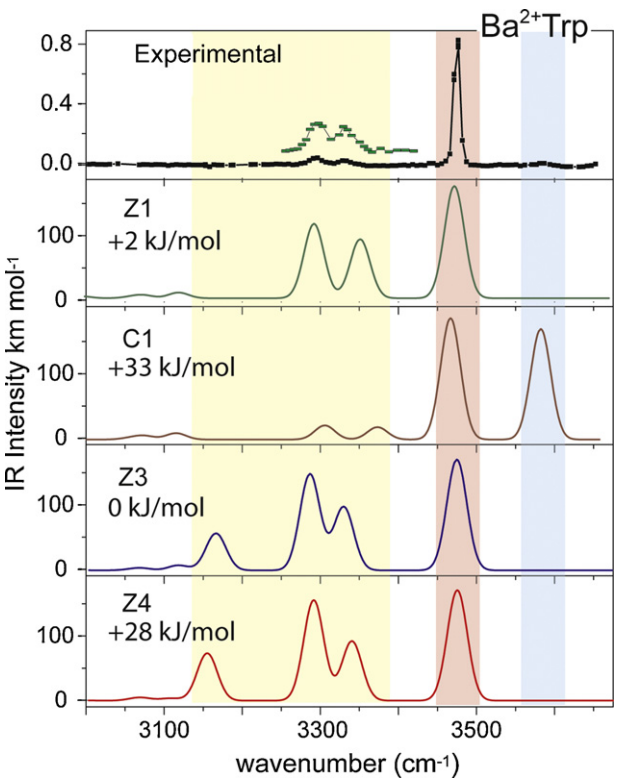

Fig. 4. IR-MPD spectrum of Ba^{2+}Trp (3000–3700 cm^{-1}) with calculated vibrational spectra for ZW (Z1, Z3, and Z4 conformations) and CS (C1 conformation). The calculated geometries are displayed in Fig. 1. Characteristic wavenumber regions of the spectrum are highlighted in yellow, red and blue to indicate the NH_3^+, indole N–H, and carboxylic acid O–H stretching modes, respectively. The zero-point corrected energies of each structure are shown for comparison. (For interpretation of references to color in this figure legend, the reader is referred to the web version of this article.)

An alternative explanation for the lack of fragmentation for the symmetric NH_3^+ stretching mode might be due to experimental constraints, including lower laser power and lower energy per photon at this wavelength. In the IR-MPD spectrum, the amine N–H stretching vibrations are reduced in intensity compared to the indole N–H stretch, as expected from the calculated linear absorption spectra. The NH_3^+ modes are likely to be more anharmonic in character than the indole N–H stretch, thus contributing to this reduction in intensity in the IR-MPD yield. The additional use of a higher-power CO_2 laser is thus found to be particularly useful to boost the IR-MPD yield of weak features in the spectrum. This approach resulted in appreciable IR-MPD yields for the weaker antisymmetric NH_3^+ bands at 3290 and 3320 cm^{-1}, approaching 25% (Fig. 3). Nonetheless, this dual-laser approach did not yield any detectable photodissociation in the symmetric NH_3^+ stretching region.

In summary, the hydrogen stretching region confirms that Ba^{2+}Trp exclusively exists in the ZW form, consistent with the presence of a predominant Z1 conformation. In fact, Ba^{2+}Trp had been investigated previously in the mid-IR region, using the free electron laser FELIX [33]. In that study, the antisymmetric CO_2^- stretch (1675 cm^{-1}) and the NH_3^+ umbrella mode (1450 cm^{-1}) yielded strong evidence for the exclusive presence of Z1, which could in fact be considered as a 'fingerprint' for the ZW structure. Similarly, the corresponding spectrum in the OPO-laser range presented here can be considered as a ZW 'fingerprint' IR-MPD spectrum, based on the lack of O–H stretching and presence of diagnostic NH_3^+ stretching modes.

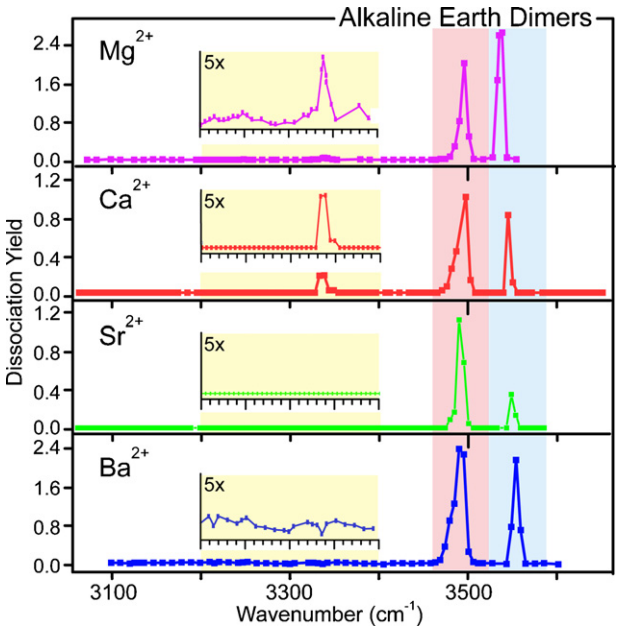

Fig. 5. IR-MPD spectra of the $M^{2+}Trp_2$ alkaline earth series in N–H and O–H stretching regions. Characteristic wavelength regions associated with NH_3^+, indole N–H, and O–H stretching modes are highlighted in yellow, red and blue, respectively. The insets show a 5 times magnification of the NH_3^+ stretching region. (For interpretation of references to color in this figure legend, the reader is referred to the web version of this article.)

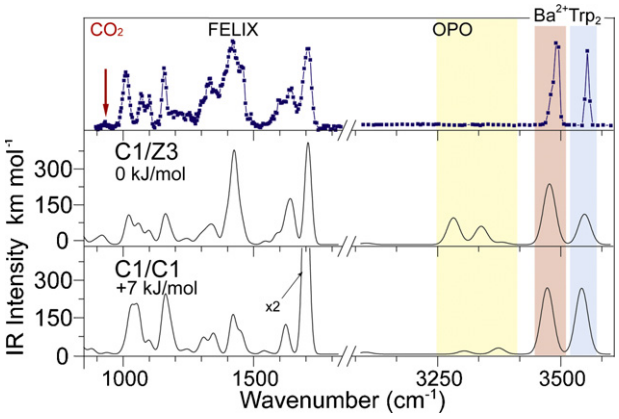

Fig. 6. IR-MPD spectra of $Ba^{2+}Trp_2$ in the mid- and near-IR regions along with calculated vibrational spectra for the two lowest-energy conformers. The calculated geometries are displayed in Fig. 2. Characteristic wavelength regions associated with NH_3^+, indole N–H, and O–H stretching modes are highlighted in yellow, red and blue, respectively. The zero-point corrected energies of each structure are shown for comparison. The CO_2 laser wavelength (10.6 μm) is indicated by a red arrow. (For interpretation of references to color in this figure legend, the reader is referred to the web version of this article.)

3.2. Alkaline earth-tryptophan dimer series

The IR-MPD spectra recorded over the 3000–3700 cm^{-1} range for a series of dimeric $M^{2+}Trp_2$ complexes (where M = Mg, Ca, Sr, and Ba) are compared in Fig. 5. All spectra exhibit intense indole N–H and carboxylic acid O–H stretches. The presence of a carboxylic acid O–H stretching band in all IR-MPD spectra confirms that at least one tryptophan is in the CS configuration. The most striking difference between the IR-MPD spectra is the presence of a weak (yet discernible) band at 3340 cm^{-1} for the $Mg^{2+}Trp_2$ and $Ca^{2+}Trp_2$ complexes (see insets), as opposed to an absence of this band in the corresponding Sr^{2+} and Ba^{2+} complexes. As all dimer complexes exhibit efficient photodissociation, the presence of this additional band indicates a structural change between smaller and larger alkaline earth complexes. Based on the $Ba^{2+}Trp$ monomer results, the most likely assignment of the 3340 cm^{-1} band is an NH_3^+ stretch mode, indicative of a ZW structure. At first sight, this suggests a mixed CS/ZW structure for $Mg^{2+}Trp_2$ and $Ca^{2+}Trp_2$, as opposed to a CS/CS configuration for the larger cation complexes, $Sr^{2+}Trp_2$ and $Ba^{2+}Trp_2$.

The structural changes are accompanied by differences in the photodissociation pathways, going from exclusive NH_3 loss for Mg^{2+} to exclusive Trp loss for Ba^{2+} (the loss of 2 NH_3 being very minor). Ca^{2+} and Sr^{2+} dimers exhibit both pathways, going from 90% NH_3 vs. 10% Trp loss for Ca^{2+}, to 60% NH_3 vs. 40% Trp loss for Sr^{2+}. This gradual shift from NH_3 loss to Trp loss is compatible with the decreasing tryptophan-(divalent metal) cation binding energy as the size of the cation increases, as shown by Dunbar et al. [7]. For the more tightly bound smaller alkaline earth cations, covalent bond cleavage leading to NH_3 loss is favored over Trp loss.

Direct correlation between dissociation pathways and molecular structure are not is straight-forward as IR-MPD spectroscopy results. Jockusch et al. had first shown a correlation between NH_3 loss (diagnostic for ZW) and H_2O loss (diagnostic for CS) channels for the alkali series bound to arginine [13], suggesting that the transition from CS to ZW occurred from Na^+ to K^+. Later spectroscopic studies by Bush et al. confirmed that the transition in fact occurs between Li^+ and Na^+ [29]. While both approaches show a qualitative agreement that smaller alkali metal complexes adopt the CS structure, as opposed to the ZW structure for larger complexes, there are differences in the quantitative analysis. The discrepancy between neutral loss branching ratios and spectroscopic results was ascribed to structural isomerization between the CS and ZW structures, which is lower in energy than covalent bond cleavage. In other words, the branching ratios in the dissociation pathways are more indicative of the transition states for the various complexes than the actual presence of particular complexes at room temperature. Similarly, in the results presented here, the branching ratios between NH_3 and Trp loss for the $M^{2+}Trp_2$ series might suggest a gradual transition from ZW-containing dimers for the smaller cations to exclusive CS configuration for the $Ba^{2+}Trp_2$ complex. The IR-MPD results seem to confirm this general trend, but indicate a more sudden transition from Ca to Sr, where no ZW conformers are confirmed for Sr.

The exclusive presence of CS/CS for the $Ba^{2+}Trp_2$ and $Sr^{2+}Trp_2$ dimers, as opposed to exclusive ZW for $Ba^{2+}Trp$ monomer seems surprising. Moreover, the trend that smaller metal cations more readily stabilize the ZW configuration, whereas larger cations do not, runs counter to most previous studies for alkali cations. The detailed spectral analysis of $Ba^{2+}Trp_2$ and $Ca^{2+}Trp_2$ complexes is shown hereafter to confirm the spectral assignments that are made. These results are also contrasted to a previous IR-MPD study using the free electron laser FELIX.

3.3. Ba^{2+} tryptophan dimer complex

Fig. 6 compares IR-MPD spectra recorded using FELIX (previous study) and the OPO-CO_2 laser scheme for $Ba^{2+}Trp_2$ with lowest-energy calculated isomers. The red arrow in the FELIX spectrum denotes the position of the fixed wavelength CO_2 laser, and confirms that $Ba^{2+}Trp_2$ does not exhibit a strong vibrational band resonant with the CO_2 laser. The same color scheme employed in Fig. 4 is shown in Fig. 6 for the carboxylic acid (blue), indole N–H (red) and NH_3^+ stretching modes (yellow).

The major difference between the $Ba^{2+}Trp_2$ and $Ba^{2+}Trp$ experimental spectra is the presence of an intense O–H stretching band (3550 cm^{-1}). This suggests that at least one tryptophan is in the CS form, and in principle allows for either CS-only or mixed CS/ZW

dimers. The calculated spectra for the lowest-energy conformers for each of these, C1/C1 and C1/Z3, are shown. In both cases, a carboxylic acid O–H stretch is predicted at 3550 cm^{-1}. The intensity of this band is intrinsically higher in the case of C1/C1, as there are two underlying oscillators, as opposed to just one in the case for C1/Z3; however, the discrimination between C1/C1 and C1/Z3 is difficult to make based on the intensity of the carboxylic acid O–H stretch band.

A more diagnostic difference between C1/C1 and C1/Z3 is seen in the intensities of their respective N–H stretching modes in the yellow region of the spectrum. Analogously to the Ba^{2+}Trp monomer, the amino NH_2 antisymmetric and symmetric stretching bands for the CS structure are much weaker in intensity than the corresponding NH_3^+ bands (10 and 30 km mol^{-1} vs. 95 and 60 km mol^{-1}). The failure to observe N–H stretching modes in the 3100–3400 cm^{-1} range suggests that neither of the tryptophans in the dimer is in the ZW form. Note that, although weak, the NH_3^+-associated bands in the more strongly bound Ba^{2+}Trp monomer in Fig. 4 (i.e., requiring covalent bond cleavage) were clearly detected. The failure to detect the loss of a tryptophan for the more weakly bound $Ba^{2+}Trp_2$, suggests that no ZW structure is present. The lower dissociation threshold of the $Ba^{2+}Trp_2$ complex is validated by observing 3 times greater fragmentation yield for the indole N–H stretch vs. the corresponding fragmentation yield for the Ba^{2+}Trp, under identical laser irradiation conditions.

In a previous FELIX IR-MPD study of $Ba^{2+}Trp_2$ (shown on the left-hand side) [7], the experimental spectrum appears to resemble the C1/Z3 calculated spectrum more closely than the C1/C1 spectrum. In that latter study, the carboxylic acid C=O and carboxylate antisymmetric CO_2^- stretch served as diagnostic peaks to distinguish between CS and ZW. Increased spectral congestion of dimer complexes resulted in spectral overlap of both diagnostic bands, which can complicate spectral interpretation. Nonetheless, since the thermochemistry predicts the complexes to be very close in energy (+7 kJ mol^{-1}), it is conceivable that different mixtures of isomers were made by ESI in both experiments. With respect to the thermochemistry results, it should be noted that the accuracy of the calculations is certainly limited. In all cases for these alkaline earth-tryptophan dimers, the mixed dimer CS/ZW is consistently predicted as the most stable configuration [7]. For $Ba^{2+}Trp_2$ this is clearly not confirmed. Moreover, the IR-MPD spectra suggest structural differences between the smaller and larger alkaline earth complexes, which are not predicted by the thermochemical results.

3.4. Ca^{2+} tryptophan dimer complex

Fig. 7 shows a comparison of the $Ca^{2+}Trp_2$ experimental spectrum recorded using FELIX [7] and the OPO laser with calculated spectra for the three lowest-energy motifs. The chemically diagnostic wavelength regions are highlighted, as previously done in Figs. 4–6. Similarly to $Ba^{2+}Trp_2$, an intense O–H stretch at 3550 cm^{-1}, associated with the carboxylic acid moiety, is observed. This again confirms that at least one tryptophan is in the CS form. However, in contrast to $Ba^{2+}Trp_2$, $Ca^{2+}Trp_2$ clearly displays an absorption band in the N–H stretching region (3340 cm^{-1}). The position of this band is consistent with an antisymmetric NH_3^+ stretching mode, diagnostic for a ZW tryptophan. The simultaneous presence of carboxylic acid O–H and NH_3^+ modes indicates the presence of a mixed CS/ZW dimer. The lowest-energy C1/Z2 and C1/Z3 mixed dimer conformations indeed confirm the presence of an antisymmetric NH_3^+ stretching mode at ~3340 cm^{-1}. Note that this band was not observed for $Ba^{2+}Trp_2$, in spite of its more efficient photodissociation. Moreover, if this band were due to an NH_2 stretch mode, associated with the CS/CS structure, then it should also have been observed for all $M^{2+}Trp_2$ complexes. These observations make a strong case for the identification of a mixed CS/ZW dimer for $Ca^{2+}Trp_2$.

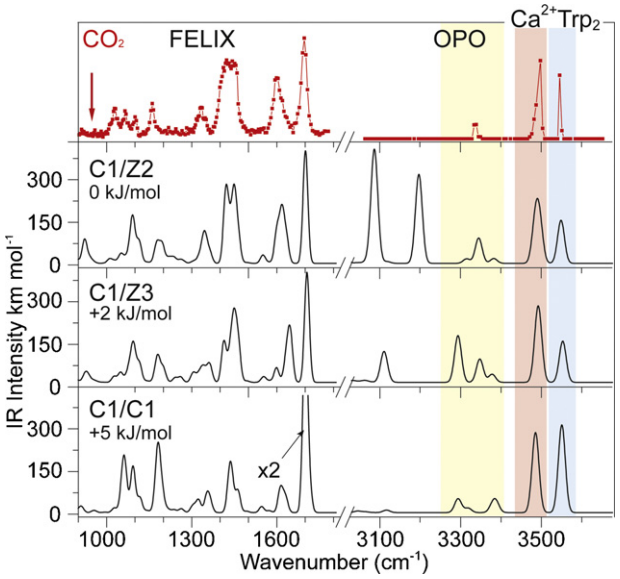

Fig. 7. IR-MPD spectra of $Ca^{2+}Trp_2$ in the mid- and near-IR regions along with calculated vibrational spectra for the three lowest-energy conformers. The calculated geometries are displayed in Fig. 2. Characteristic wavelength regions associated with NH_3^+, indole N–H, and O–H stretching modes are highlighted in yellow, red and blue, respectively. The zero-point corrected energies of each structure are shown for comparison. The CO_2 laser wavelength (10.6 μm) is indicated by a red arrow. (For interpretation of references to color in this figure legend, the reader is referred to the web version of this article.)

Intriguingly though, other intense NH_3^+ stretches that are predicted at lower-frequency are not observed. The calculations indicate that the exact position of these lower-frequency NH_3^+ modes are highly dependent on conformation. While C1/Z2 predicts NH_3^+ stretches at 3090 and 3195 cm^{-1}, the marginally higher-energy structure C1/Z3 (+2 kJ mol^{-1}) predicts the corresponding modes at 3110 and 3295 cm^{-1}. On the other hand, the higher-frequency NH_3^+ stretch at 3340 cm^{-1} is consistently reproduced at the same frequency for both geometries. In higher-energy conformations (not shown here), the same trend is observed, in that the position of the antisymmetric NH_3^+ stretch is unaffected by conformation, whereas the lower-frequency bands are. Given the floppy nature of these complexes at room temperature, it is thus conceivable that the lower-frequency NH_3^+ bands are not as well defined as the antisymmetric NH_3^+ stretch. If such structures were to interconvert at room temperature or during infrared activation, this would impede resonant absorption of multiple photons for such NH_3^+ stretching modes from OPO-laser irradiation. Resonant absorption of multiple photons may, however, be required to reach the quasi-continuum, where non-resonant absorption from CO_2 laser irradiation brings the ions over the dissociation threshold. Another contributing factor to lower IR-MPD yield is likely to be the lower energy per photon, as well as lower laser power than for the corresponding antisymmetric NH_3^+ stretch.

Despite the inability to detect multiple NH_3^+ modes, the appearance of a band at 3340 cm^{-1} suggests the presence of a ZW configuration for one of the tryptophans, and is consistent with a mixed CS/ZW dimer. This does, however, not exclude the possibility of CS/CS dimers, which may also be present at some level. The previous FELIX study on $Ca^{2+}Trp_2$ was also compatible with a CS/ZW configuration [7]. In this case, C1/Z2 yielded a better match with the experimental spectrum than C1/Z3. No such distinction could be established in the OPO-laser range, due to an inability to detect the lower-frequency NH_3^+ modes.

3.5. Metal binding effects on ZW stabilization

The size effect to favor ZW-containing tryptophans for smaller cations runs counter to the trend established by Jockusch et al. [13,17] and Bush et al. [29] for arginine bound to the alkali metal series (Li^+–Cs^+), and later confirmed by Armentrout for serine and methione [27,32]. On the other hand, IR spectroscopy results on cationized proline by Schäfer and co-workers [55] showed an opposite trend in the stabilization of ZW for smaller alkali metals, as opposed to CS for larger cations. Schäfer hypothesized that this trend should be mainly observed in aliphatic amino acids, which lack a functionalized side-chain (e.g., heteroatom N, O, S, or aromatic ring). Such functionalized side-chains offer binding partners for the metal cations, whereas the aliphatic amino acids, such as proline (glycine, alanine, valine, leucine and isoleucine), are limited to binding via their amino N or acid O moieties. In the absence of competing side-chain binding partners, the larger polarizing effect of smaller metal cations leads to charge separation (i.e., ZW structure).

In our case of tryptophan dimers, the rationale above cannot explain the effects that are observed, since tryptophan is not an aliphatic amino acid. The question thus arises what other factors are responsible. From chemical intuition, in dimer complexes steric effects are likely to play a much more pronounced role than in monomer complexes. The binding patterns considered for $M^{2+}Trp_2$ are summarized in Fig. 2. In C1/C1, the lowest-energy CS-only geometry, the metal engages in electrostatic bonding to the carboxylic acid O, amino N, and the indole side-chain π-cloud on both tryptophans. This results in a large degree of steric crowding around the cation, and is hence only favored for larger cations, such as Sr^{2+} and Ba^{2+}. Conversely, this binding motif is not compatible for the smaller cations, Mg^{2+} and Ca^{2+}. Those would favor the lowest-energy mixed dimer conformation, C1/Z2. In the latter conformation, Z2 adopts a more extended form, where the carboxylate is tightly solvated, whereas the indole side-chain is not involved in binding to the metal cation. The more compact mixed dimer conformation, C1/Z3, where the cation binds to both indole side-chains, is probably less favored in smaller alkaline earth complexes, due to steric crowding, as in fact confirmed by the computations. It is not clear why C1/Z3 would be disfavored relative C1/C1 for larger cations. Single-point MP2 calculations for C1/Z3 and C1/C1 (not shown) did not show considerable differences in stability between both geometries, indicating that dispersion interactions do not explain this observation. In summary, the mixed dimer extended structure, C1/Z2, is consistent with solvating a smaller cation, whereas the more compact CS-only conformation, C1/C1, requires a larger cation, to minimize steric repulsion.

4. Conclusions

It is shown that the N–H and O–H stretching regions serve as a useful 'fingerprint' region in identifying ZW or CS structure in the gas phase. The structural assignment is based on diagnostic bands associated with the carboxylic acid OH stretch (CS) and the NH_3^+ asymmetric stretching mode (ZW). A clear example of a ZW structure is observed for monomeric Ba^{2+}Trp, by virtue of a lack of photodissociation between 3525 and 3625 cm^{-1} (O–H) and the presence of a doublet at 3290 cm^{-1} and 3320 cm^{-1} (N–H). The simple distinction of these two wavelength regions is then implemented on tryptophan dimer complexes for the alkaline earth series. An unexpected trend is seen, in that the CS/ZW mixed structure is favored with decreasing metal size, as opposed to CS/CS for larger cations (Sr^{2+} and Ba^{2+}). This trend is in sharp contrast to other studies on alkali metal-chelated amino acids. These results point to the complex interplay of forces that determine Zwitterion stabilization in the gas-phase, showing that trends are not always easy to generalize. In this case, it is hypothesized that steric effects account for differences in stability between CS/CS and CS/ZW isomers. A more extended CS/ZW structure, not involving the ZW indole side-chain, is capable of effectively solvating smaller alkaline earth cations. Conversely, the more tightly bound CS/CS structure involves both indole side-chains, and hence presents steric crowding problems for smaller cations. For larger cation complexes, these steric effects are less of a concern.

Acknowledgements

NP thanks the University of Florida for generous start-up funds. The OPO laser was funded from an In-House Research Program (IHRP) grant to JRE from the National High Magnetic Field Laboratory (NHMFL). WKM was partially supported by the NSF-PIRE (OISE-0730072) grant; WLP was partially supported by the IHRP grant and by the National Science Foundation (CHE-0718007). The FT-ICR mass spectrometer was funded by the National Science Foundation Major Research Instrumentation Program. This material is based upon work supported by the National Science Foundation under CHE-0845450.

References

[1] B.A. Wallace, Common structural features in gramicidin and other ion channels, BioEssays 22 (2000) 227–234.
[2] D.A. Doyle, J.M. Cabral, R.A. Pfuetzner, A. Kuo, J.M. Gulbis, S.L. Cohen, B.T. Chait, R. MacKinnon, The structure of the potassium channel: molecular basis of K^+ conduction and selectivity, Science 280 (1998) 69.
[3] P. Venkataraman, R.A. Lamb, L.H. Pinto, Chemical rescue of histidine selectivity filter mutants of the M2 ion channel of influenza a virus, J. Biol. Chem. 280 (2005) 21463–21472.
[4] M. Cotten, C. Tian, D.D. Busath, R.B. Shirts, T.A. Cross, Modulating dipoles for structure–function correlations in the Gramicidin A channel, Biochemistry 38 (1999) 9185–9197.
[5] W. Hu, T.A. Cross, Tryptophan hydrogen bonding and electric dipole moments: functional roles in the gramicidin channel and implications for membrane proteins, Biochemistry 34 (1995) 14147–14155.
[6] D. Buck, NMDA channel gating is influenced by a tryptophan residue in the M2 domain but calcium permeation is not altered, Biophys. J. 79 (2000) 2454–2462.
[7] R.C. Dunbar, J.D. Steill, N.C. Polfer, J. Oomens, Dimeric complexes of tryptophan with M^{2+} metal ions, J. Phys. Chem. A 113 (2009) 845–851.
[8] J. Oomens, B.G. Sartakov, G. Meijer, G. von Helden, Gas-phase infrared multiple photon dissociation spectroscopy of mass-selected molecular ions, Int. J. Mass Spectrom. 254 (2006) 1–19.
[9] N.C. Polfer, J. Oomens, Vibrational spectroscopy of bare and solvated ionic complexes of biological relevance, Mass Spectrom. Rev. 28 (2009) 468–494.
[10] T.D. Fridgen, Infrared consequence spectroscopy of gaseous protonated and metal ion cationized complexes, Mass Spectrom. Rev. 28 (2009) 586–607.
[11] M. Schäfer, M.K. Drayss, D. Blunk, J.M. Purcell, C.L. Hendrickson, A.G. Marshall, A. Mookherjee, P.B. Armentrout, Kinetic determination of potassium affinities by IRMPD: elucidation of precursor ion structures, J. Phys. Chem. A 113 (2009) 7779–7783.
[12] C. Kapota, J. Lemaire, P. Maitre, G. Ohanessian, Vibrational signature of charge solvation vs salt bridge isomers of sodiated amino acids in the gas phase, J. Am. Chem. Soc. 126 (2004) 1836–1842.
[13] R.A. Jockusch, W.D. Price, E.R. Williams, Structure of cationized arginine ($Arg.M^+$, M = H, Li, Na, K, Rb, and Cs) in the gas phase: further evidence for zwitterionic arginine, J. Phys. Chem. A 103 (1999) 9266–9274.
[14] N.C. Polfer, J. Oomens, D.T. Moore, G. von Helden, G. Meijer, R.C. Dunbar, Infrared spectroscopy of phenylalanine Ag(I) and Zn(II) complexes in the gas phase, J. Am. Chem. Soc. 128 (2006) 517–525.
[15] N.C. Polfer, J. Oomens, R.C. Dunbar, IRMPD spectroscopy of metal-ion/tryptophan complexes, Phys. Chem. Chem. Phys. 8 (2006) 2744–2751.
[16] J.M. Talley, B.A. Cerda, G. Ohanessian, C. Wesdemiotis, Alkali metal ion binding to amino acids versus their methyl esters: affinity trends and structural changes in the gas phase, Chem. Eur. J. 8 (2002) 1377–1388.
[17] M.W. Forbes, M.F. Bush, N.C. Polfer, J. Oomens, R.C. Dunbar, E.R. Williams, R.A. Jockusch, Infrared spectroscopy of arginine cation complexes: direct observation of gas-phase zwitterions, J. Phys. Chem. A 111 (2007) 11759–11770.
[18] N.C. Polfer, B. Paizs, L.C. Snoek, I. Compagnon, S. Suhai, G. Meijer, G. von Helden, J. Oomens, Infrared fingerprint spectroscopy and theoretical studies of potassium ion tagged amino acids and peptides in the gas phase, J. Am. Chem. Soc. 127 (2005) 8571–8579.
[19] M.M. Kish, G. Ohanessian, C. Wesdemiotis, The Na^+ affinities of [alpha]-amino acids: side-chain substituent effects, Int. J. Mass Spectrom. 227 (2003) 509–524.

[20] T. Marino, N. Russo, M. Toscano, Interaction of Li^+, Na^+, and K^+ with the proline amino acid. Complexation modes potential energy profiles, and metal ion affinities, J. Phys. Chem. B 107 (2003) 2588–2594.
[21] T. Shoeib, K.W.M. Siu, A.C. Hopkinson, Silver ion binding energies of amino acids: use of theory to assess the validity of experimental silver ion basicities obtained from the kinetic method, J. Phys. Chem. A 106 (2002) 6121–6128.
[22] A.S. Lemoff, M.F. Bush, E.R. Williams, Binding energies of water to sodiated valine and structural isomers in the gas phase: the effect of proton affinity on zwitterion stability, J. Am. Chem. Soc. 125 (2003) 13576–13584.
[23] A.S. Lemoff, M.F. Bush, E.R. Williams, Structures of cationized proline analogues: evidence for the zwitterionic form, J. Phys. Chem. A 109 (2005) 1903–1910.
[24] A.S. Lemoff, M.F. Bush, C. Wu, E.R. Williams, Structures and hydration enthalpies of cationized glutamine and structural analogues in the gas phase, J. Am. Chem. Soc. 127 (2005) 10276–10286.
[25] B.A. Cerda, C. Wesdemiotis, Gas phase copper(I) ion affinities of valine, lysine, and arginine based on the dissociation of Cu^+-bound heterodimers at varying internal energies, Int. J. Mass Spectrom. 185–187 (1999) 107–116.
[26] A. Lesarri, E.J. Cocinero, J.C. López, J.L. Alonso, The shape of neutral valine, Angew. Chem. Int. Ed. 43 (2004) 605–610.
[27] P.B. Armentrout, M.T. Rodgers, J. Oomens, J.D. Steill, Infrared multiphoton dissociation spectroscopy of cationized serine: effects of alkali-metal cation size on gas-phase conformation, J. Phys. Chem. A 112 (2008) 2248–2257.
[28] M.T. Rodgers, P.B. Armentrout, J. Oomens, J.D. Steill, Infrared multiphoton dissociation spectroscopy of cationized threonine: effects of alkali-metal cation size on gas-phase conformation, J. Phys. Chem. A 112 (2008) 2258–2267.
[29] M.F. Bush, J.T. O'Brien, J.S. Prell, R.J. Saykally, E.R. Williams, Infrared spectroscopy of cationized arginine in the gas phase: direct evidence for the transition from nonzwitterionic to zwitterionic structure, J. Am. Chem. Soc. 129 (2007) 1612–1622.
[30] M.F. Bush, J.S. Prell, R.J. Saykally, E.R. Williams, One water molecule stabilizes the cationized arginine zwitterion, J. Am. Chem. Soc. 129 (2007) 13544–13553.
[31] M.F. Bush, J. Oomens, E.R. Williams, Proton affinity zwitterion stability new results from infrared spectroscopy and theory of cationized lysine and analogues in the gas phase, J. Phys. Chem. A 113 (2009) 431–438.
[32] D.R. Carl, T.E. Cooper, J. Oomens, J.D. Steill, P.B. Armentrout, Infrared multiple photon dissociation spectroscopy of cationized methionine: effects of alkali-metal cation size on gas-phase conformation, Phys. Chem. Chem. Phys. 12 (2010) 3384–3398.
[33] R.C. Dunbar, N.C. Polfer, J. Oomens, Gas-phase zwitterion stabilization by a metal dication, J. Am. Chem. Soc. 129 (2007) 14562–14563.
[34] M.F. Bush, J. Oomens, R.J. Saykally, E.R. Williams, Alkali metal ion binding to glutamine and glutamine derivatives investigated by infrared action spectroscopy and theory, J. Phys. Chem. A 112 (2008) 8578–8584.
[35] K. Rajabi, T.D. Fridgen, Structures of aliphatic amino acid proton-bound dimers by infrared multiple photon dissociation spectroscopy in the 700–2000 cm^{-1} region, J. Phys. Chem. A 112 (2008) 23–30.
[36] R. Wu, T.B. McMahon, Infrared multiple photon dissociation spectra of proline and glycine proton-bound homodimers. Evidence for zwitterionic structure, J. Am. Chem. Soc. 129 (2007) 4864–4865.
[37] M.F. Bush, J. Oomens, R.J. Saykally, E.R. Williams, Effects of alkaline earth metal ion complexation on amino acid zwitterion stability: results from infrared action spectroscopy, J. Am. Chem. Soc. 130 (2008) 6463–6471.
[38] H. Oh, C. Lin, H.Y. Hwang, H. Zhai, K. Breuker, V. Zabrouskov, B.K. Carpenter, F.W. McLafferty, Infrared photodissociation spectroscopy of electrosprayed ions in a Fourier transform mass spectrometer, J. Am. Chem. Soc. 127 (2005) 4076–4083.
[39] X. Kong, I. Tsai, S. Sabu, C. Han, Y.T. Lee, H. Chang, S. Tu, A.H. Kung, C. Wu, Progressive stabilization of zwitterionic structures in $[H(Ser)_{2-8}]^+$ studied by infrared photodissociation spectroscopy, Angew. Chem. Int. Ed. 45 (2006) 4130–4134.
[40] J.R. Roscioli, L.R. McCunn, M.A. Johnson, Quantum structure of the intermolecular proton bond, Science 316 (2007) 249–254.
[41] J.M. Headrick, Spectral signatures of hydrated proton vibrations in water clusters, Science 308 (2005) 1765–1769.
[42] R. Walters, T. Jaeger, M. Duncan, Infrared spectroscopy of $Ni^+(C_2H_2)_{(n)}$ complexes: evidence for intracluster cyclization reactions, J. Phys. Chem. A 106 (2002) 10482–10487.
[43] M.A. Duncan, Structures, energetics and spectroscopy of gas phase transition metal ion–benzene complexes, Int. J. Mass Spectrom. 272 (2008) 99–118.
[44] J.M. Lisy, Spectroscopy and structure of solvated alkali-metal ions, Int. Revs. Phys. Chem. 16 (1997) 267–289.
[45] J.M. Lisy, Infrared studies of ionic clusters: the influence of Yuan T. Lee, J. Chem. Phys. 125 (2006) 132302.
[46] D.J. Goebbert, T. Wende, R. Bergmann, G. Meijer, K.R. Asmis, Messenger-tagging electrosprayed ions: vibrational spectroscopy of suberate dianions, J. Phys. Chem. A 113 (2009) 5874–5880.
[47] J.T. O'Brien, J.S. Prell, J.D. Steill, J. Oomens, E.R. Williams, Changes in binding motif of protonated heterodimers containing valine and amines investigated using IRMPD spectroscopy between 800 and 3700 cm^{-1} and theory, J. Am. Chem. Soc. 131 (2009) 3905–3912.
[48] T. Rizzo, J. Stearns, O. Boyarkin, Spectroscopic studies of cold, gas-phase biomolecular ions, Int. Rev. Phys. Chem. 28 (2009) 481–515.
[49] E.B. Cagmat, J. Szczepanski, W.L. Pearson, D.H. Powell, J.R. Eyler, N.C. Polfer, Vibrational signatures of metal-chelated monosaccharide epimers: gas-phase infrared spectroscopy of Rb^+-tagged glucuronic and iduronic acid, Phys. Chem. Chem. Phys. 12 (2010) 3474–3479.
[50] L.I. Yeh, J.M. Price, Y.T. Lee, Infrared spectroscopy of the pentacoordinated carbonium ion $C_2H_7^+$, J. Am. Chem. Soc. 111 (1989) 5597–5604.
[51] D.M. Peiris, M.A. Cheeseman, R. Ramanathan, J.R. Eyler, Infrared multiple photon dissociation spectra of gaseous ions, J. Phys. Chem. 97 (1993) 7839–7843.
[52] J.J. Valle, J.R. Eyler, J. Oomens, D.T. Moore, A.F.G. van der Meer, G. von Helden, G. Meijer, C.L. Hendrickson, A.G. Marshall, G.T. Blakney, Free electron laser-Fourier transform ion cyclotron resonance mass spectrometry facility for obtaining infrared multiphoton dissociation spectra of gaseous ions, Rev. Sci. Instrum. 76 (2005) 023103.
[53] M. Frisch, G. Trucks, H. Schlegel, G. Scuseria, M. Robb, J. Cheeseman, J. Montgomery, T. Vreven, K. Kudin, J. Burant, J. Millam, S. Iyengar, J. Tomasi, V. Barone, B. Mennucci, M. Cossi, G. Scalmani, N. Rega, G. Petersson, H. Nakatsuji, M. Hada, M. Ehara, K. Toyota, R. Fukuda, J. Hasegawa, M. Ishida, T. Nakajima, Y. Honda, O. Kitao, H. Nakai, M. Klene, X. Li, J. Knox, H. Hratchian, J. Cross, V. Bakken, C. Adamo, J. Jaramillo, R. Gomperts, R. Stratmann, O. Yazyev, A. Austin, R. Cammi, C. Pomelli, J. Ochterski, P. Ayala, K. Morokuma, G. Voth, P. Salvador, J. Dannenberg, V. Zakrzewski, S. Dapprich, A. Daniels, M. Strain, O. Farkas, D. Malick, A. Rabuck, K. Raghavachari, J. Foresman, J. Ortiz, Q. Cui, A. Baboul, S. Clifford, J. Cioslowski, B. Stefanov, G. Liu, A. Liashenko, P. Piskorz, I. Komaromi, R. Martin, D. Fox, T. Keith, M. Al-Laham, C. Peng, A. Nanayakkara, M. Challacombe, P. Gill, B. Johnson, W. Chen, M. Wong, C. Gonzalez, J. Pople, Gaussian 03, Revision B.03, Gaussian Inc., Wallingford, CT, USA, 2004.
[54] J.P. Merrick, D. Moran, L. Radom, An evaluation of harmonic vibrational frequency scale factors, J. Phys. Chem. A 111 (2007) 11683–11700.
[55] M.K. Drayß, P. Armentrout, J. Oomens, M. Schäfer, IR spectroscopy of cationized aliphatic amino acids: stability of charge-solvated structure increases with metal cation size, Int. J. Mass Spectrom. 297 (2010) 18–27.